HHS Public Access

Author manuscript

Magn Reson Imaging Clin N Am. Author manuscript; available in PMC 2017 February 01.

Published in final edited form as:

Magn Reson Imaging Clin N Am. 2016 February ; 24(1): 123–133. doi:10.1016/j.mric.2015.08.011.

Evaluation of head and neck tumors with functional MRI

Jacobus F.A. Jansen, Ph.D.[1], **Carlos Parra, Ph.D.**[2], **Yonggang Lu, Ph.D.**[3], and **Amita Shukla-Dave, Ph.D.**[2,4]

Jacobus F.A. Jansen: jacobus.jansen@mumc.nl; Carlos Parra: carlos.parra@gmail.com; Yonggang Lu: ylu@radonc.wustl.edu; Amita Shukla-Dave: davea@mskcc.org

[1]Department of Radiology, Maastricht University Medical Center, Maastricht, The Netherlands [2]Department of Medical Physics, Memorial Sloan-Kettering Cancer Center, New York, NY, USA [3]Department of Radiation Oncology, University of Washington, St Louis, USA [4]Department of Radiology, Memorial Sloan-Kettering Cancer Center, New York, NY, USA

Synopsys

Head and neck (HN) cancer is one of the most common cancers worldwide. Magnetic Resonance Imaging (MRI) based diffusion and perfusion techniques enable the non-invasive assessment of tumor biology and physiology, which supplement information obtained from standard structural scans. Diffusion and perfusion MRI techniques provide novel biomarkers that can aid the monitoring pre-, during, and post-treatment stages to improve patient selection for therapeutic strategies, provide evidence for change of therapy regime, and evaluation of treatment response. This review discusses pertinent aspects of the role of diffusion and perfusion MRI and computational analysis methods in studying HN cancer.

Keywords

Head and neck cancer; MRI; diffusion; perfusion; data processing

Discussion of Problem/Clinical Presentation

Head and Neck (HN) cancer is one of the major types of cancer, affecting 50,000 new patients in the US every year [1]. HN cancers typically originate from the mucosal epithelia of the oral cavity, pharynx, and larynx and can be linked to alcohol consumption and tobacco smoking [2]. For early HN cancers, encouraging locoregional control can be reached through radiation or surgery treatment. However, for advanced HN cancer the odds are less favorable, as with standard therapy only 60% of patients will survive 5 years [1]. HN cancers frequently metastasize to (cervical) lymph nodes before they penetrate distant organs such as the lungs. In spite of recent advances in surgical and oncologic treatments, the overall

Corresponding author: Jacobus F.A. Jansen[1] Ph.D., Assistant Professor, Department of Radiology, Maastricht University Medical Center, PO Box 5800, 6202 AZ Maastricht, The Netherlands, Phone: +31 (0) 43 387 4908, jacobus.jansen@mumc.nl.

survival rate of patients with HN cancer has unfortunately not improved much over recent years [1]. Important causes for unfavorable outcome in advance HN cancer can be a delayed diagnosis (followed by loco regional failure) and a tardy salvage treatment at the recurrence of the disease. A priori predictors of outcome and predictive biomarkers of treatment response are desperately needed to advance patient care and individualized treatment. For example, non-invasive imaging biomarkers could have an important role in the clinical decision-making process, thereby allowing oncologists to use interventions with alternative therapy strategies. Imaging has several benefits as a method for improving the tumor treatment evaluation, as it can sample the entire tumor non-invasively, it can be repeated longitudinally to monitor changes at regular intervals.

Functional MRI might provide the ideal tools yielding such non-invasive markers [3,4]. This review will focus on the promises of diffusion and perfusion weighted MRI techniques in HN cancer. Diffusion Weighted -MRI (DW-MRI) can quantify and map the diffusion of molecules (typically water), in biological tissues [5], whereas perfusion MRI can assess the passage of blood through vessels through tissue [6,7]. Both MRI techniques have a rich history that extends decades, and the MRI tools available to assess the associated processes are currently on a very mature level, providing excellent opportunities to study both diffusion and perfusion in HN cancer. Although some might consider MR spectroscopy also to be a functional MRI technique, it falls beyond the scope of this review, and we would like to refer the reader to an excellent review by Abdel Razek et al. [8].

Diffusion

Diffusion Weighted Imaging (DWI) is a MR technique that allows the measurement of water self-diffusivity [5]. Since freedom of motion of water molecules is hindered by interactions with other molecules and cellular barriers, water molecule diffusion abnormalities can reflect changes of tissue organization at the cellular level (e.g. increase of extracellular space due to cell death). These micro-structural changes affect the (hindered) motion of water molecules, and consequently alter the water diffusion properties and thus the MR signal. Apart from deriving a measure for the average extent of molecular motion that is affected by cellular organization and integrity (apparent diffusion coefficient, ADC), it is also possible using Diffusion Tensor Imaging (DTI, in which diffusion is measured in several directions) to measure the preferred direction of molecular motion, which provides information on the degree of alignment of cellular structures, as well as their structural integrity (fractional anisotropy, FA). Recently, also DWI techniques have entered the HN cancer clinic, in which images are acquired with multiple b-values, yielding techniques such as intravoxel incoherent imaging (IVIM) [9] or diffusion kurtosis imaging (DKI) [10], techniques that aim to provide information that extends diffusion of water, such as perfusion (for IVIM) or non-Gaussian diffusion behavior (for DKI).

Perfusion

Perfusion is physiologically defined as the steady-state delivery of blood to tissue [6,7]. Two major approaches exist to assess perfusion with MRI. The first is the application of an exogenous contrast agent (usually a gadolinium-based), exploiting the susceptibility effects or relaxivity effects of the contrast agents on the signal, respectively dynamic susceptibility

contrast-enhanced (DSC) MR perfusion or dynamic contrast-enhanced (DCE) MR perfusion. The second application involves the use of an endogenous contrast agent, namely magnetically labeled arterial blood water, as a diffusible flow tracer in arterial spin labeling (ASL) MR perfusion. Especially DCE, and to a lesser extend ASL are currently being used to study HN cancer.

Outline

The present narrative review summarizes recent literature and provides an overview of the various studies in which diffusion or perfusion based MRI studies are applied to HN cancer. This review is structured as follows; it will first provide an overview of commonly used acquisition protocols and postprocessing methods, followed by advanced data analysis, imaging findings regarding tumor characterization and differentiation, tumor risk stratification and staging, monitoring and prediction of treatment response. Subsequently, limitations will be highlighted followed by a conclusion with recommendations for future research.

Imaging protocols

1. DW-MRI

Data acquisition

- **MRI scanner and coil:** DW-MRI studies for head and neck cancers are commonly carried out on 1.5T or 3T MRI scanners using dedicated neurovascular phase array coils [10–12].
- **Pulse sequence:** Clinical DW-MRI is most commonly performed using single-shot spin-echo EPI, axial, free breathing.
- **Acquisition parameters (see** table 1): Protocol optimization is a prerequisite for obtaining optimum signal to noise in DWI images. The number of b-values for mono exponential modeling of the data are 2–3 and the b values >100 s/mm^2; (usually between 500–1200 s/mm^2) while the number of b values increase up to 10 or more (usually between 0–1500 s/mm^2) including both the high and low b values for bi-exponential modeling of the data [9,10,13]; Slice thickness: 5–8 mm, Gap thickness: 0 mm, Field of view: 200–380 mm [14]; acquired Matrix: 128 × 128 or higher [5]; Number of averages: 2–4; Parallel imaging (SENSE or ASSET): Factor= 2; TE: Ideal/Target: minimum TE; Acceptable: <110 ms; TR: 2–4s; Receiver Bandwidth: >1000 Hz/voxel.

DW-MRI Data processing

- **Region of Interest Analysis:** The regions of interest (ROIs) are usually drawn on the DW-MR images by an experienced neuroradiologist based on the radiological and clinical information. The ROI encompasses the entire tumor and node of interest.
- **Quantitative methods:** Mono- and bi-exponential models [9,10,13,15] are usually used for quantifying diffusion either on the basis of voxel by voxel or based on the

region of interest. For mono-exponential model, apparent diffusion coefficient (ADC) value can be quantified using S/S0 = exp(−b×ADC), where S and S0 are the signal intensities with and without diffusion weighting, respectively, and b is the gradient factor (b value, s/mm^2) [11,15]. For bi-exponential model [9,16], metrics related to intravoxel incoherent motions can be calculated using

$$S=S_0((1-f)\exp(-bD)+f\exp(-bD^*))$$

or

$$S=S_0((1-f)\exp(-bD+\frac{1}{6}b^2D^2K)+f\exp(-bD^*)),$$

where f is the vascular volume fraction or perfusion factor, D is the pure diffusion coefficient (mm^2/s), D^* is the pseudo-diffusion coefficient (mm^2/s) associated with blood velocity and capillary geometry, and K is the diffusion kurtosis coefficient. Noise floor rectification schemes are commonly used in the above diffusion quantifications [17].

2. DCE-MRI Data acquisition

- **MRI scanner and coil:** DCE-MRI studies for head and neck cancers are commonly being carried out on 1.5T or 3T MRI scanners using dedicated neurovascular phase array coils.
- **Contrast agent:** The most commonly used contrast agent is paramagnetic gadolinium chelates, such as Gd-DTPA (gadopentetic diethylenetriamine pentaacetic acid) (Magnevist; Berlex Laboratories, Wayne, NJ, USA) [18–20]. The bolus of contrast agent is typically delivered at 0.1mmol/kg body weight at 2 cc/s, followed by a 20 ml saline flush with a flow rate of 2 cc/s using a MR-compatible, programmable power injector (e.g., Spectris; Medrad, Indianola, PA, USA) [20–22].
- **Pulse sequence:** Most of the DCE-MRI data acquisition is performed using a fast 2D or 3D gradient-echo sequence due to its high T_1-sensitivity and rapid image acquisition [18–20]. A 3D spoiled gradient-echo (3D-SPGR) sequence is more widely applied than 2D-SPGR because of its ability to achieve higher spatial resolution and signal-to-noise ratio (SNR).
- **Acquisition parameters (see** table 1): The acquisition parameters can be tailored depending on whether the study design needs higher spatial resolution or higher temporal resolution. Typical parameters on GE MR scanners are: FOV~=22 cm, TR ~= 5.3 ms, TE ~= 1.4 ms, temporal resolution ~= 4 s, phases ~= 50, NEX = 1. Temporal resolution ranges from 3 to 6 s and acquisition time is generally in the range of 2 to 10 minutes [18,20,23].

DCE-MRI Data processing

- **RF field inhomogeneity correction:** Radiofrequency (RF) field non-uniformities often cause inhomogeneity in image profile. Image correction methods, such as an edge-completed low pass filter algorithm, can be used to correct this kind of image artifacts [19]. Additionally, this inhomogeneity can result in deviation of the flip angles from nominal values when using gradient-echo sequences for data acquisition. This flip angle deviation has a great impact on the calculation of native T_1 relaxation time values, further influencing the accuracies of the estimated pharmacokinetic parameters. A double-echo method can be used to correct this artifact [24,25].

- **Motion artifact correction:** DCE-MRI images in the head and neck region suffer from motion artifacts due to the voluntary and involuntary motions of patients. The motions can cause in-plane and through-plane image artifacts. Image registration methods are commonly used to correct the through-plane image artifacts by realigning the DCE-MRI time-series image itself or co-registering DCE-MRI images with other image modalities, such as T_1- or T_2-weighted images [18,19,26]. Rigid body alignments are more readily performed than non-rigid deformations [19].

DCE-MRI Data quantification

- **Semi-quantitative methods:** Semi-quantitative methods classify the signal intensity time curve of DCE-MRI into different patterns or provide some simple summary descriptors about the curve. For curve pattern classification, the initial enhancement (1–2 min) of the curve is usually described as fast, medium, and slow uptake. The late enhancement (>2 min) of the curve is often classified as persistent, plateau, and washout [27]. Normal tissues and tumor tissues with different degrees of malignancy could show different curve patterns. This feature can be used for tumor detection and tumor differentiation [28,29]. For curve summary description, several summary parameters, such as maximum *contrast index* (CI), time to reach maximum CI, maximum slope, washout slope, area under the curve at a specific time (e.g., AUC90 means the area under the curve at 90 s after contrast injection), are used [6,19].

- **Pharmacokinetic modeling methods:** Pharmacokinetic modeling methods provide characteristics of tumor microvasculature (related to endothelial permeability, the size of extracellular extravascular space (EES), and the size of intravascular space) by modeling tumor contrast kinetics into separate compartments and establishing the transport equation of the contrast agent. Commonly used models are the *Tofts model*, *extended Tofts model*, *shutter speed model* (SSM), and the *two compartment exchange model* (2CXM) [18,20,26,30,31]. Among these models, the Tofts model is mostly used. From the Tofts model, kinetic parameters such as K^{trans} (volume transfer rate between vascular space and EES, min^{-1}) and v_e (volume fraction of the EES) can be characterized on a basis of tumor region of interest (ROI) or voxel-by-voxel [18–20]. For these models, accurate estimation of the arterial input function (AIF) is required, and when this is not

possible in individual cases, also averaged population based AIF functions can be used [23].

3. ASL-MRI Data acquisition

- **MRI scanner and coil:** ASL-MRI studies for head and neck cancers[32,33] have been reported using 3T MRI scanners using dedicated neurovascular phase array coils.
- **Pulse sequence:**

  ASL can be acquired with a sequence using echo-planar MRI signal targeted by alternating radiofrequency (RF) pulses (EPI STAR)[32]. Magnetic labeling of in-flowing arterial blood can be achieved using section-selective 180° RF pulses in labeling slab. After the labeling, a Look–Locker readout of gradient-echo EPI with an excitation pulse of 30° can be used for image acquisition. Additionally control images without labeling need to be acquired. Also PCASL (Pseudo-Continuous Arterial Spin Labeling) techniques have been reported[34]. The acquisition of pCASL can be performed by using multishot spin-echo echo-planar imaging to obtain control and labeled images. The labeling slab can be placed just under the bifurcation of the internal and external carotid arteries.

  Acquisition parameters (see table 1): Typical parameters on 3.0T Philips MR scanners for EPI STAR are: TR, 3000 ms; TE, 24 ms; FOV, 230×230 mm; 80×80 matrix; slice thickness, 10 mm; interslice gap, 30%; NEX 30. Label slab of 58.5-mm-thick located 20 mm proximal to the imaging section. For pCASL parameters are as follows: labeling duration, 1650 ms; postlabel delay, 1280 ms; TR, 3619 ms; TE, 18 ms; flip angle, 90°; number of shots, 2; field of view (FOV), 230× 230 mm; matrix, 80× 80; slice thickness, 5 mm; number of slices, 15; acceleration factor for parallel imaging, 2.

ASL Data quantification

- Tumor blood flow (TBF) can be calculated using image processing software such as MatLab (MathWorks, Natick, MA). TBF can be calculated from analysis of magnetization difference (DM) obtained by subtracting the labeled images from the ASL control images [32,34]. TBF maps can be created on a pixel-by-pixel basis.

Advanced data analysis—In addition to using perfusion or diffusion based MRI contrasts for a better evaluation of HN cancer, also on the data analysis side developments to improve the applicability of MR images in HN cancer are currently going on. Most of these techniques do not need specific MRI contrasts is input, as in principle they work on any quantitative map. For example, the parametric response map (PRM) approach [35], is a voxel-based approach that allows segmentation of a tumor volume on the base of regional intratumoral changes in the MR signal. It is ideally suited to accurately follow treatment induced changes in tumors on a voxel-by-voxel basis. Another analysis method allows for accurate assessment of tumor heterogeneity. HN cancer can be very heterogeneous in nature, as the tumor vascular system is typically chaotic and poorly organized, and tumor

heterogeneity itself is a well-recognized feature that is associated with tumor malignancy [36]. In particular, tumor heterogeneity in the blood supply may prevent therapeutic efficacy and result in treatment resistance. Therefore, tumor heterogeneity may play an important role in assessing tumor malignancy and predicting treatment response. Most studies typically use summarizing characteristics, such as mean, median, or standard deviation of voxelwise measures, to describe the nature of the whole tumor volume. However, these commonly used measures do not necessarily reflect the marked morphologic heterogeneity in nodal metastases of head and neck cancer. Image texture analysis may be an ideal candidate to assess tumor tissue heterogeneity in a reliable manner [37–39]. In texture analysis, an algorithm that assesses spatial intensity coherence is applied to an image yielding several textural features (reflecting heterogeneity), independent of the image's mean and variance. The gray-level co-occurrence matrix (GLCM), or gray-level spatial dependence matrix, constitutes one of the most important algorithms used for texture analysis [40].

Imaging findings

1). Tumor characterization and differentiation

Studies have shown that DW-MRI and DCE-MRI can be used to differentiate different tumor types. Sumi et al [41] combined use of IVIM and time-signal intensity curve (TIC) analyses to diagnose head and neck tumors. IVIM parameters (f and D values) and TIC profiles in combination were distinct among the different types of head and neck tumors, including squamous cell carcinomas (SCCs), lymphomas, malignant salivary gland tumors, Warthin's tumors, pleomorphic adenomas and schwannomas and a multi-parametric approach using both measures differentiated between benign and malignant tumors with 97% accuracy and diagnosed different tumor types with 89% accuracy. A combined use of IVIM parameters and TIC profiles may have high efficacy in diagnosing head and neck tumors.

Lee et al used DCE-MRI–derived parameters to differentiate squamous cell carcinoma (SCC), undifferentiated carcinoma (UD), and lymphoma; they showed that K_{trans}, AUC60, and AUC90 were significantly different between UD/SCC and UD/lymphoma, but not between SCC/lymphoma [6].

Similarly, Asaumi et al [42] attempted to differentiate malignant lymphomas from SCCs using DCE-MRI with 17 lesions of malignant lymphoma and 30 cases of SCC. The results showed that there was a significant difference between SCC and malignant lymphoma in the time to reach the maximum contrast index (CI).

Fong et al [43] showed that DW-MRI was successful in 45/65 with nasopharynx (NPC), 5/7 with lymphoma and 26/28 with SCC and the mean ADC (+/−SD) of NPC, lymphoma and SCC were 0.98+/−0.161, 0.75+/−0.190, 1.14+/−0.196 ($\times 10(^{-3})$mm(2)/s) respectively which were significantly different ($p<0.001$–0.003).

Srinivasan et al in their DWI study found that head and neck squamous cell cancer (HNSCC) patients had a significantly lower mean ADC value (1.101 (+/−0.214) $\times$ $10(^{-3})$ $mm(^{2})$/s) than paraspinal muscles, pterygoid muscle, masseter muscle, thyroid gland, and

base of the tongue (P=0.0006, 0.0002, 0.0001, 0.001, and 0.002, respectively). The tumor ADC values were not significantly different from ADC values of parotid and submandibular glands (P=0.057 and 0.14, respectively) [14]. In their another study with 33 patients at 3T MR scanner, they found that there was a statistically significant difference (P = .004) between the mean ADC values (in $10(^{-3})$ $mm(^{2})/s$) in the benign and malignant lesions (1.505 +/− 0.487; 95% confidence interval, 1.305–1.706, and 1.071 +/− 0.293; 95% confidence interval, 0.864–1.277, respectively), and suggested that a 3T ADC value of 1.3×10^{-3} mm^2/s may be the threshold value for differentiation between benign and malignant head and neck lesions [44].

2). Tumor risk stratification and staging

In a recent study by Lu et al [15], they evaluated the utility of DW-MRI as a novel pre-operative tool for risk stratification in thyroid cancer. The study concludes that ADC values of papillary thyroid cancers (PTCs) with extrathyroidal extension (ETE; $1.53\pm0.25\times10^{-3}$,mm^2/s) were significantly lower than corresponding values from PTCs without ETE ($2.37\pm0.67\times10^{-3}$ mm^2/s; $p<0.005$) and the cutoff ADC was determined at 1.85×10^{-3} mm^2/s with a sensitivity of 85%, specificity of 85%, and ROC curve area of 0.85. that had extra thyroidal extension (ETE) from those patients that did not have ETE. ETE was assessed at pathology making DW-MRI a tool of choice for pre-operative clinical workup.

Vandecaveye et al, investigated the role of DWI in nodal staging in HNSCC patients [45]. In their study, DW imaging led to a correct change in nodal stage for 12 (36%) of 33 patients: The nodal stage of two patients was downgraded: from N1 to N0 in one patient and from N2b to N0 in the other. In four patients, a contralateral metastasis that was initially undetected at preoperative MR imaging was diagnosed at DW imaging. The nodal stage of the lymph node in the neck of six patients was upgraded from N0 to N1 or N2b in three patients with laryngeal cancer, to N2b in two patients with tongue cancer, and to ipsilateral metastasis in one patient with mouth floor cancer. In this patient with mouth floor cancer, a contralateral lymph node at neck level 2 that was considered suspicious at TSE (turbo spin-echo imaging) was correctly diagnosed as benign at DW imaging, and the extent of the contralateral neck dissection was consequently reduced. Compared with TSE, DW imaging performed with ADCb0-1000 values had higher accuracy than MR imaging in nodal staging, providing added value in the detection of sub-centimeter nodal metastases.

3) Monitoring of treatment response

To evaluate diffusion-weighted imaging (DWI) for assessment of early treatment response in HNSCC after the end of chemoradiotherapy (CRT), Vandecaveye V et al found that the ΔADC (the ADC change between pretreatment and after treatment) of lesions with later tumor recurrence was significantly lower than lesions with complete remission for both primary lesions (−2.3% ± 0.3% vs. 80% ± 41%; $p < 0.0001$) and adenopathies (19.9% ± 32% vs. 63% ± 36%; $p = 0.003$). The ΔADC showed a PPV of 89% and an NPV of 100% for primary lesions and a PPV of 70% and an NPV of 96% for adenopathies per neck side. DWI improved PPV and NPV compared to anatomical imaging [12].

Kim S et al investigated the ADC change in 40 newly diagnosed HNSCC patients before, during, and after the end of chemoradiation therapy, and found that pretreatment ADC value of complete responders ($1.04 +/- 0.19 \times 10^{-3}$ mm^2/s) was significantly lower ($P < 0.05$) than that from partial responders ($1.35 +/- 0.30 \times 10^{-3}$ mm^2/s). A significant increase in ADC was observed in complete responders within 1 week of treatment ($P < 0.01$), which remained high until the end of the treatment. The complete responders also showed significantly higher increase in ADC than the partial responders by the first week of chemoradiation ($P < 0.01$). These results suggest that ADC can be used as a marker for early detection of response to concurrent chemoradiation therapy in HNSCC [11]. See figure 1.

4). Prediction of treatment response

Shukla-Dave et al [20] showed in a DCE-MRI study performed on 74 HNSCC patients that in a stepwise Cox regression, skewness of K_{trans} (volume transfer constant) was the strongest predictor for Stage IV patients (progression free survival and overall survival: $p < 0.001$). This study suggests an important role for pretreatment DCE-MRI in prediction of outcome in these patients.

Baer et al [35] reported the utility of DCE-MRI in assessment of treatment response. They showed in ten patients with loco-regionally HNSCC who underwent definitive concurrent chemoradiation therapy that the volume transfer constant and normalized area under the contrast-enhancement time curve at 60 seconds were predictive of survival both in parametric response map analysis (volume transfer constant, P= .002; normalized area under the contrast-enhancement time curve at 60 seconds, P = .02) and in the percentage change analysis (volume transfer constant, P = .04; normalized area under the contrast-enhancement time curve at 60 seconds, P= .02). After appropriate validation this method may find use in potentially guide treatment modification in patients with predicted treatment failure.

A study was performed on 37 HNSCC patients undergoing induction chemotherapy (IC) by Bernstein et al [46] and the median baseline tumor plasma flow (F_p) was 53.2 ml/100 ml/min in 25 responders and 23.9 in 12 non-responders ($P = 0.027$). Median baseline F_p in lymph nodes was 25.8 ml/100 ml/min for 37 nodes in 25 responders and 17.1 for 15 nodes in 12 non-responders ($p = 0.066$) and frequency of IC response in 37 patients was 68% overall, 83% for tumor F_p above the median (40.6 ml/100 ml/min) and 45% below the median. Thereby concluding that pre-treatment tumor F_p determined by DCE–MRI predicts IC response in HNSCC.

In a recent study, by Fujima et al [32], using arterial spin labeling (ASL) in twenty-two patients with head and neck cancer were evaluated perfusion measures before and after nonsurgical treatment. The study showed that the tumor blood flow (TBF) reduction rate was significantly lower in patients with residual tumors (0.54±0.12) than in those without (0.85±0.06) and thereby ASL technique could accurately determine the effect of nonsurgical treatment. See figure 2.

In a feasibility IVIM study on neck nodal metastases by Hauser et al [47] in 15 HNSCC patients who received radiotherapy in combination with chemotherapy and/or immunotherapy it was shown that the initial perfusion fraction (f) value was significantly

higher (p = 0.01) in patients with LRF compared to patients with locoregional control (LRC). LRF was present in three patients only. These preliminary findings need to be further validated.

Noij et al [48] performed pretreatment MRI on 78 HNSCC patients and ADC as well as contrast enhanced (CE) T1weighted images (WI) were evaluated and the results exhibited that tumor volume(sensitivity:73%; specificity: 57%) and lymph node ADC_{1000} (sensitivity: 71–79%; specificity:77–79%) were independent significant predictors of disease free survival without and with including CE-T1WI ($P < 0.05$).

In their HNSCC study, Srinivasan et al found that a significant difference ($P = 0.03$) in mean ADC between patients showing positive and negative outcomes (1.18 and $1.43 * 10^{-3}$ mm2/s, respectively), and patients with lower pretreatment ADC and with greater than 45% of volume below ADC threshold of 1.15×10^{-3} mm2/s may have better outcome to chemoradiation at 2 years [44].

Lu et al[49] assessed the merits of texture analysis on parametric maps derived from pharmacokinetic modeling with DCE-MRI for the prediction of treatment response in patients with HNSCC. In this retrospective study, 19 HNSCC patients underwent pre- and intra-treatment DCE-MRI scans at a 1.5T MRI scanner. Image texture analysis was then employed on maps of K_{trans} and v_e, generating two texture measures: energy (E) and homogeneity (H). No significant changes were found for the mean and standard deviation for K_{trans} and v_e ($p>0.09$), however texture analysis revealed that the imaging biomarker energy (E) of v_e was significantly higher in intra-treatment scans, relative to pretreatment scans ($p<0.04$). See figure 3.

Pearls, Pitfalls, and Variants

Functional MRI techniques such as diffusion and perfusion MRI allow for quantifying tumor characteristics related to tumor cellularity and vascularity. Compared to anatomical imaging techniques such as T1W and T2W MRI, functional MRI techniques have shown their added values in tumor detection, characterization, staging, treatment response monitoring and prediction. However, there are a number of limitations for these techniques. In DCE-MRI, patient voluntary and involuntary motion is a major source of error in the derived metrics of tumor tissues, therefore, images should be motion corrected before further analysis. The nonspecific nature of vessel leakage can lead to high false-negative and false-positive results which require other imaging modalities to correctly interpret tumor characteristics. Lack of standardized protocols is another issue which needs consideration to compare the results in different studies. Moreover, the use of individual and population AIF is another source of variability among different studies. In DWI, DWI images suffer from patient motions and susceptibility difference in head and neck cancers. b-value selection is crucial to the ADC quantification since too low and too high b-values can lead to inaccurate estimation of ADC values. For IVIM and its variant modeling fitting, perfusion metrics are highly sensitive to image noise, thereby limiting the benefits of such techniques. Therefore, to enable clinical applications of DW-MRI and DCE-MRI in head and neck cancers, the experiments of DW-MRI and DCE-MRI should be carefully designed, standardized,

implemented and interpreted. Overall, for most of the discussed techniques, in addition to state of the art dedicated MRI hardware, also dedicated software and especially knowledgeable personnel is needed to obtain reliable data that can be used in the clinic.

Summary/Conclusions

Considering the diversity of applications and demonstrated potential of diffusion and perfusion imaging methods, the importance of these techniques in assessing HN cancer is expected to grow. Until now, most studies reporting on MRI diffusion and perfusion in HN cancer included relatively small populations (i.e. $n < 100$), but this is likely to increase in the future. To obtain reliable biomarkers that extend beyond standard structural scans, however, one has to consider potential complicating factors, with respect to both the data acquisition and processing. Yet, most problems have been critically addressed and can be taken into account in a satisfying manner. Also, further progress in the development of (for example automated) analysis methods has to be stimulated to make diffusion and perfusion imaging procedures more easily (i.e. push button) applicable in clinical routine.

Acknowledgments

Drs. Parra and Shukla-Dave are supported by the National Cancer Institute/National Institutes of Health (grant number 1 R21CA176660-01A1).

References

1. Jemal A, Siegel R, Xu J, Ward E. Cancer statistics, 2010. CA: a cancer journal for clinicians. 2010; 60:277–300. [PubMed: 20610543]
2. Vokes EE, Weichselbaum RR, Lippman SM, Hong WK. Head and neck cancer. The New England journal of medicine. 1993; 328:184–94. [PubMed: 8417385]
3. Jansen JF, Koutcher JA, Shukla-Dave A. Non-invasive imaging of angiogenesis in head and neck squamous cell carcinoma. Angiogenesis. 2010; 13:149–60. [PubMed: 20383743]
4. Stephen RM, Gillies RJ. Promise and progress for functional and molecular imaging of response to targeted therapies. Pharmaceutical research. 2007; 24:1172–85. [PubMed: 17385018]
5. Chawla S, Kim S, Wang S, Poptani H. Diffusion-weighted imaging in head and neck cancers. Future oncology. 2009; 5:959–75. [PubMed: 19792966]
6. Lee FK, King AD, Ma BB, Yeung DK. Dynamic contrast enhancement magnetic resonance imaging (DCE-MRI) for differential diagnosis in head and neck cancers. Eur J Radiol. 2011
7. Noij DP, de Jong MC, Mulders LG, et al. Contrast-enhanced perfusion magnetic resonance imaging for head and neck squamous cell carcinoma: a systematic review. Oral Oncol. 2015; 51:124–38. [PubMed: 25467775]
8. Abdel Razek AA, Poptani H. MR spectroscopy of head and neck cancer. Eur J Radiol. 2013; 82:982–9. [PubMed: 23485098]
9. Lu Y, Jansen JF, Mazaheri Y, Stambuk HE, Koutcher JA, Shukla-Dave A. Extension of the intravoxel incoherent motion model to non-gaussian diffusion in head and neck cancer. J Magn Reson Imaging. 2012; 36:1088–96. [PubMed: 22826198]
10. Jansen JF, Stambuk HE, Koutcher JA, Shukla-Dave A. Non-gaussian analysis of diffusion-weighted MR imaging in head and neck squamous cell carcinoma: A feasibility study. AJNR Am J Neuroradiol. 2010; 31:741–8. [PubMed: 20037133]
11. Kim S, Loevner L, Quon H, et al. Diffusion-weighted magnetic resonance imaging for predicting and detecting early response to chemoradiation therapy of squamous cell carcinomas of the head and neck. Clinical cancer research : an official journal of the American Association for Cancer Research. 2009; 15:986–94. [PubMed: 19188170]

12. Vandecaveye V, Dirix P, De Keyzer F, et al. Diffusion-weighted magnetic resonance imaging early after chemoradiotherapy to monitor treatment response in head-and-neck squamous cell carcinoma. Int J Radiat Oncol Biol Phys. 2012; 82:1098–107. [PubMed: 21514067]
13. Yuan J, Yeung DK, Mok GS, et al. Non-Gaussian analysis of diffusion weighted imaging in head and neck at 3T: a pilot study in patients with nasopharyngeal carcinoma. PloS one. 2014; 9:e87024. [PubMed: 24466318]
14. Lambrecht M, Vandecaveye V, De Keyzer F, et al. Value of diffusion-weighted magnetic resonance imaging for prediction and early assessment of response to neoadjuvant radiochemotherapy in rectal cancer: preliminary results. Int J Radiat Oncol Biol Phys. 2012; 82:863–70. [PubMed: 21398048]
15. Lu Y, Moreira AL, Hatzoglou V, et al. Using Diffusion-Weighted MRI to Predict Aggressive Histological Features in Papillary Thyroid Carcinoma: A Novel Tool for Pre-Operative Risk Stratification in Thyroid Cancer. Thyroid. 2015
16. Lu Y, Jansen JF, Stambuk HE, et al. Comparing primary tumors and metastatic nodes in head and neck cancer using intravoxel incoherent motion imaging: a preliminary experience. J Comput Assist Tomogr. 2013; 37:346–52. [PubMed: 23674004]
17. Prah DE, Paulson ES, Nencka AS, Schmainda KM. A simple method for rectified noise floor suppression: Phase-corrected real data reconstruction with application to diffusion-weighted imaging. Magn Reson Med. 2010; 64:418–29. [PubMed: 20665786]
18. Kim S, Loevner LA, Quon H, et al. Prediction of response to chemoradiation therapy in squamous cell carcinomas of the head and neck using dynamic contrast-enhanced MR imaging. AJNR Am J Neuroradiol. 2010; 31:262–8. [PubMed: 19797785]
19. Noworolski SM, Fischbein NJ, Kaplan MJ, et al. Challenges in dynamic contrast-enhanced MRI imaging of cervical lymph nodes to detect metastatic disease. J Magn Reson Imaging. 2003; 17:455–62. [PubMed: 12655585]
20. Shukla-Dave A, Lee NY, Jansen JF, et al. Dynamic Contrast-Enhanced Magnetic Resonance Imaging as a Predictor of Outcome in Head and Neck Squamous Cell Carcinoma Patients with Nodal Metastases. Int J Radiat Oncol Biol Phys. 2011
21. Chawla S, Kim S, Loevner LA, et al. Prediction of disease-free survival in patients with squamous cell carcinomas of the head and neck using dynamic contrast-enhanced MR imaging. AJNR Am J Neuroradiol. 2011; 32:778–84. [PubMed: 21349969]
22. Jansen JF, Schoder H, Lee NY, et al. Tumor Metabolism and Perfusion in Head and Neck Squamous Cell Carcinoma: Pretreatment Multimodality Imaging With (1)H Magnetic Resonance Spectroscopy, Dynamic Contrast-Enhanced MRI, and [(18)F]FDG-PET. Int J Radiat Oncol Biol Phys. 2012; 82:299–307. [PubMed: 21236594]
23. Shukla-Dave A, Lee N, Stambuk H, et al. Average arterial input function for quantitative dynamic contrast enhanced magnetic resonance imaging of neck nodal metastases. BMC Med Phys. 2009; 9:4. [PubMed: 19351382]
24. Stollberger R, Wach P. Imaging of the active B1 field in vivo. Magn Reson Med. 1996; 35:246–51. [PubMed: 8622590]
25. Wang J, Qiu M, Yang QX, Smith MB, Constable RT. Measurement and correction of transmitter and receiver induced nonuniformities in vivo. Magn Reson Med. 2005; 53:408–17. [PubMed: 15678526]
26. Kim S, Quon H, Loevner LA, et al. Transcytolemmal water exchange in pharmacokinetic analysis of dynamic contrast-enhanced MRI data in squamous cell carcinoma of the head and neck. J Magn Reson Imaging. 2007; 26:1607–17. [PubMed: 17968962]
27. Schnall MD, Ikeda DM. Lesion Diagnosis Working Group report. J Magn Reson Imaging. 1999; 10:982–90. [PubMed: 10581516]
28. Kusunoki T, Murata K, Nishida S, Tomura T, Inoue M. Histopathological findings of human thyroid tumors and dynamic MRI. Auris Nasus Larynx. 2002; 29:357–60. [PubMed: 12393041]
29. Tunca F, Giles Y, Salmaslioglu A, et al. The preoperative exclusion of thyroid carcinoma in multinodular goiter: Dynamic contrast-enhanced magnetic resonance imaging versus ultrasonography-guided fine-needle aspiration biopsy. Surgery. 2007; 142:992–1002. discussion e1–2. [PubMed: 18063087]

30. Donaldson SB, Betts G, Bonington SC, et al. Perfusion estimated with rapid dynamic contrast-enhanced magnetic resonance imaging correlates inversely with vascular endothelial growth factor expression and pimonidazole staining in head-and-neck cancer: a pilot study. Int J Radiat Oncol Biol Phys. 2011; 81:1176–83. [PubMed: 21546171]
31. Machiels JP, Henry S, Zanetta S, et al. Phase II study of sunitinib in recurrent or metastatic squamous cell carcinoma of the head and neck: GORTEC 2006-01. J Clin Oncol. 2010; 28:21–8. [PubMed: 19917865]
32. Fujima N, Kudo K, Yoshida D, et al. Arterial spin labeling to determine tumor viability in head and neck cancer before and after treatment. J Magn Reson Imaging. 2014; 40:920–8. [PubMed: 25356468]
33. Fujima N, Nakamaru Y, Sakashita T, et al. Differentiation of squamous cell carcinoma and inverted papilloma using non-invasive MR perfusion imaging. Dento maxillo facial radiology. 2015:20150074. [PubMed: 26054571]
34. Fujima N, Kudo K, Tsukahara A, et al. Measurement of tumor blood flow in head and neck squamous cell carcinoma by pseudo-continuous arterial spin labeling: comparison with dynamic contrast-enhanced MRI. J Magn Reson Imaging. 2015; 41:983–91.
35. Baer AH, Hoff BA, Srinivasan A, Galban CJ, Mukherji SK. Feasibility analysis of the parametric response map as an early predictor of treatment efficacy in head and neck cancer. AJNR Am J Neuroradiol. 2015; 36:757–62. [PubMed: 25792532]
36. Jackson A, O'Connor JP, Parker GJ, Jayson GC. Imaging tumor vascular heterogeneity and angiogenesis using dynamic contrast-enhanced magnetic resonance imaging. Clinical cancer research : an official journal of the American Association for Cancer Research. 2007; 13:3449–59. [PubMed: 17575207]
37. Alic L, van Vliet M, van Dijke CF, Eggermont AM, Veenland JF, Niessen WJ. Heterogeneity in DCE-MRI parametric maps: a biomarker for treatment response? Phys Med Biol. 2011; 56:1601–16. [PubMed: 21335648]
38. Alic L, van Vliet M, Wielopolski PA, et al. Regional heterogeneity changes in DCE-MRI as response to isolated limb perfusion in experimental soft-tissue sarcomas. Contrast media & molecular imaging. 2013; 8:340–9. [PubMed: 23613437]
39. Davnall F, Yip CS, Ljungqvist G, et al. Assessment of tumor heterogeneity: an emerging imaging tool for clinical practice? Insights into imaging. 2012; 3:573–89. [PubMed: 23093486]
40. McNitt-Gray MF, Wyckoff N, Sayre JW, Goldin JG, Aberle DR. The effects of co-occurrence matrix based texture parameters on the classification of solitary pulmonary nodules imaged on computed tomography. Computerized medical imaging and graphics : the official journal of the Computerized Medical Imaging Society. 1999; 23:339–48. [PubMed: 10634146]
41. Sumi M, Nakamura T. Head and neck tumours: combined MRI assessment based on IVIM and TIC analyses for the differentiation of tumors of different histological types. European radiology. 2014; 24:223–31. [PubMed: 24013848]
42. Asaumi J, Yanagi Y, Konouchi H, Hisatomi M, Matsuzaki H, Kishi K. Application of dynamic contrast-enhanced MRI to differentiate malignant lymphoma from squamous cell carcinoma in the head and neck. Oral Oncol. 2004; 40:579–84. [PubMed: 15063385]
43. Fong D, Bhatia KS, Yeung D, King AD. Diagnostic accuracy of diffusion-weighted MR imaging for nasopharyngeal carcinoma, head and neck lymphoma and squamous cell carcinoma at the primary site. Oral Oncol. 2010; 46:603–6. [PubMed: 20619723]
44. Srinivasan A, Chenevert TL, Dwamena BA, et al. Utility of pretreatment mean apparent diffusion coefficient and apparent diffusion coefficient histograms in prediction of outcome to chemoradiation in head and neck squamous cell carcinoma. J Comput Assist Tomogr. 2012; 36:131–7. [PubMed: 22261783]
45. Vandecaveye V, De Keyzer F, Vander Poorten V, et al. Head and neck squamous cell carcinoma: value of diffusion-weighted MR imaging for nodal staging. Radiology. 2009; 251:134–46. [PubMed: 19251938]
46. Bernstein JM, Kershaw LE, Withey SB, et al. Tumor plasma flow determined by dynamic contrast-enhanced MRI predicts response to induction chemotherapy in head and neck cancer. Oral Oncol. 2015; 51:508–13. [PubMed: 25700703]

47. Hauser T, Essig M, Jensen A, et al. Prediction of treatment response in head and neck carcinomas using IVIM-DWI: Evaluation of lymph node metastasis. Eur J Radiol. 2014; 83:783–7. [PubMed: 24631600]

48. Noij DP, Pouwels PJ, Ljumanovic R, et al. Predictive value of diffusion-weighted imaging without and with including contrast-enhanced magnetic resonance imaging in image analysis of head and neck squamous cell carcinoma. Eur J Radiol. 2015; 84:108–16. [PubMed: 25467228]

49. Lu, Y.; Jansen, JF.; Gupta, G., et al. Prediction of treatment response using texture analysis on pharmacokinetic maps of dynamic contrast enhanced MRI in patients with head and neck cance. Joint Annual Meeting ISMRM-ESMRMB 2014; Milan, Italy. 2014; p. 4076

Key points

- Functional MRI techniques (diffusion and perfusion MRI) allow for quantifying tumor characteristics related to tumor physiology and biology
- Compared to anatomical imaging techniques, functional MRI techniques have shown their added value in (head and neck) HN tumor detection, characterization, staging, treatment response monitoring and prediction
- Dedicated MRI hardware, software, and knowledgeable personnel is essential to obtain reliable data and to translate to the HN clinic

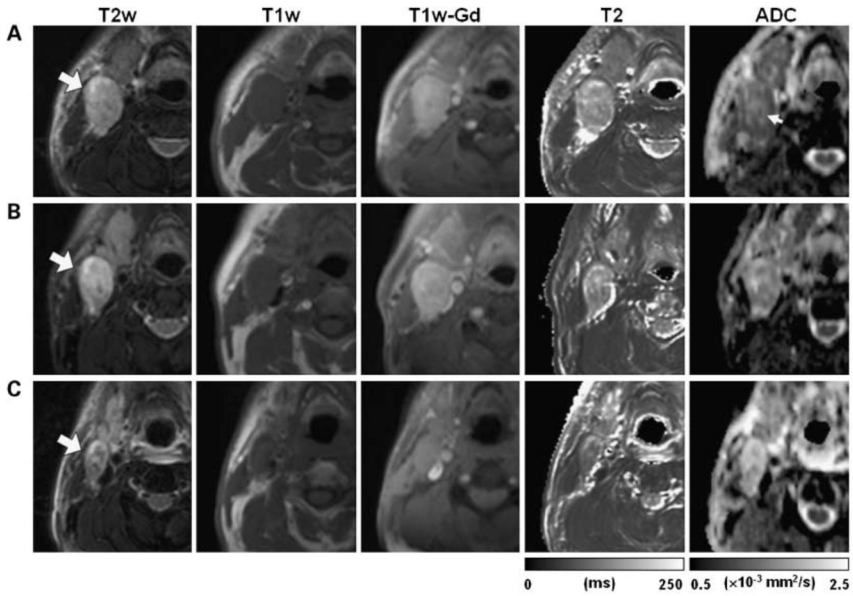

Figure 1.

Array of representative images of a HNSCC patient with partial response after treatment. Images in each row are from three measurement time points: pretreatment (A), 1 week after radiation therapy (B), and 2 weeks after the completion of the treatment (C). *Large arrows*, same metastatic nodal mass that was followed through the treatment course; *small arrow*, central region of the mass with ADC higher than the rim. (From Kim S, Loevner L, Quon H, et al. Diffusion-weighted magnetic resonance imaging for predicting and detecting early response to chemoradiation therapy of squamous cell carcinomas of the head and neck. Clinical cancer research : an official journal of the American Association for Cancer Research 2009;15:986–94, with permission.)

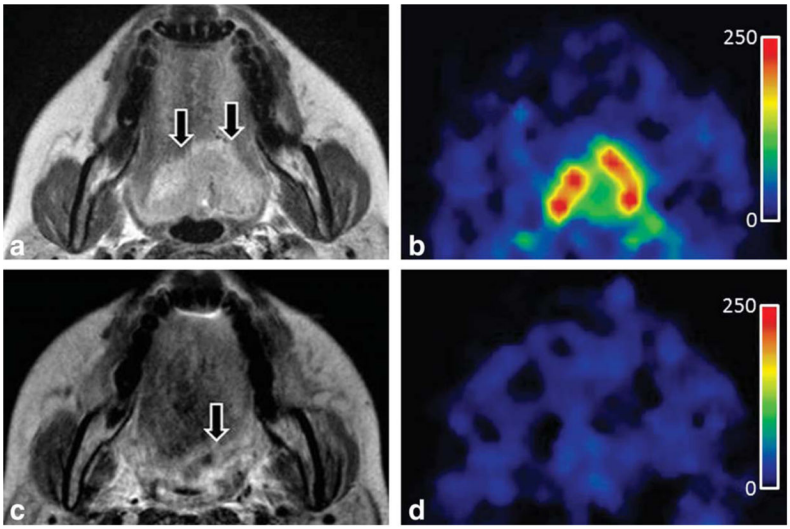

Figure 2.

T2-weighted and ASL-derived (tumor blood flow) TBF maps of a patient (41-year-old female) with tongue cancer, before (a,b) and after (c,d) treatment. (b) Pretreatment TBF map shows high blood flow corresponding to the primary lesion. (d) The posttreatment TBF map shows that higher blood flow is not observed in the PTC area compared to the surrounding soft tissue. The 12-month follow-up confirmed that this lesion was not a residual tumor. (From Fujima N, Kudo K, Yoshida D, et al. Arterial spin labeling to determine tumor viability in head and neck cancer before and after treatment. J Magn Reson Imaging 2014;40:920–8, with permission.)

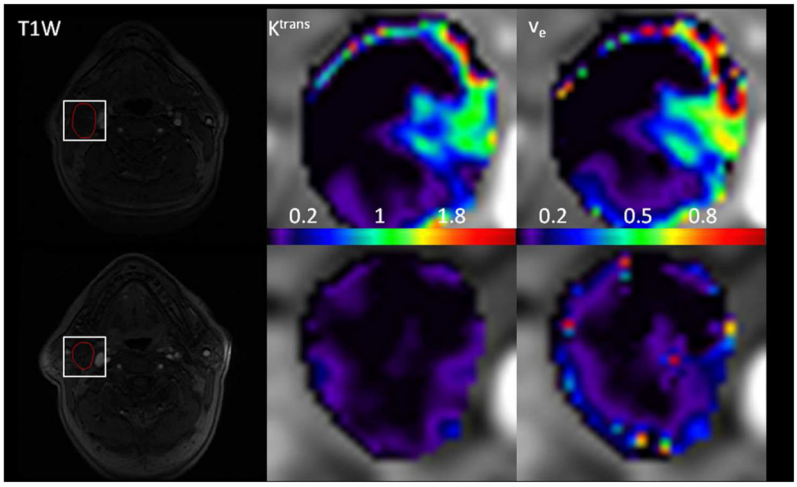

Figure 3.

Pretreatment and intra-treatment DCE-MRI images of (a) a patient with locoregional control (male, 63y). The top row shows pretreatment images, and the bottom row shows images from the intra-treatment stage. From left to right, the columns show a T1-weighted image, K^{trans} (min^{-1}) map, and v_e map. The white rectangles delineate the regions of interest (ROIs) at the metastatic nodes. K^{trans} and v_e maps are zoomed at the locations of ROIs (data is from the authors' clinic).

Table 1

typical acquisition parameters

Contrast	Sequence	TE/TR (ms)	Slice thickness (mm)	FOV (mm)	Matrix	Extras
DW-MRI	Single-shot spin-echo EPI	<110/2000–4000	5–8	200–380	≥ 128×128	>2 b-values, 0–1500 s/mm^2
DCE-MRI	3D spoiled gradient-echo	~1.4/5.3	5–8	~220	≥ 128×128	Gd-DTPA bolus 0.1mmol/kg body weight at 2 cc/s, followed by a 20 ml saline flush Temporal resolution: 3–6 s; ~50 phases
ASL	Multishot spin-echo echo-planar, PCASL	~20/4000	5	~230	~80×80	labeling duration: 1650 ms; postlabel delay: 1280 ms; 2 shots; labeling just under the bifurcation

DW-MRI: diffusion weighted MRI; DCE-MRI: Dynamic contrast enhanced MRI; ASL: arterial spin labeling; EPI: echo planar imaging; PCASL: Pseudo-Continuous Arterial Spin Labeling; TE: echo time; TR repetition